Physics – Uspekhi **54** (11) 1117 – 1130 (2011)

REVIEWS OF TOPICAL PROBLEMS

PACS numbers: **62.50. – p**, 75.30.Kz, 75.40.Cx, 77.80.B –

Itinerant helimagnet MnSi

S M Stishov, A E Petrova

DOI: 10.3367/UFNe.0181.201111b.1157

Contents

Abstract. Manganese silicide (MnSi), a model helimagnetic compound, crystallizes in a B20 structure, whose non-centrosymmetric space group $P2_13$ allows a helical (chiral) magnetic structure. The magnetic phase transition temperature of MnSi (29 K at atmospheric pressure) decreases with pressure and approaches zero at about 1.4 GPa. This fact, pointing to possible quantum critical phenomena, has prompted high-pressure studies of MnSi that have revealed a number of fascinating phenomena, in particular, the non-Fermi-liquid behavior of electrical resistivity and the unusual spin state (partial ordering) in the paramagnetic phase. We discuss experimental results characterizing the physical properties and the phase diagram of MnSi and at the same time forming the basis of current ideas in the physics of strongly correlated chiral electron systems.

1. Introduction

The intermetallic compound MnSi (manganese silicide) belongs to the class of weak itinerant-electron (band) magnets with a low Curie temperature and small magnetic moment (a few fractions of the Bohr magneton). This class also includes compounds such as FeGe, $Fe_{1-x}Co_xSi$, $ZrZn_2$, Ni_3Al, Ni_3Y, Ni_3Ga, Sc_3Al, and CoS_2. The magnetic susceptibility of these compounds in the paramagnetic phase approximately obeys the Curie–Weiss law, with the effective magnetic moment in the paramagnetic phase significantly exceeding the magnetic moment derived from the saturation magnetization.

In contrast to other substances mentioned above, MnSi, FeGe, and $Fe_{1-x}Co_xSi$ compounds are helimagnets (have a helical magnetic structure), which to a significant extent determines the variety of observed physical phenomena and separates these materials from the class of weak band magnets. But because MnSi has been studied the most of all these compounds (which is largely due to the availability of high-quality single crystals), it is the description of its properties that became the subject of numerous theories and concepts stimulating the development of new experiments. In fact, MnSi is a model substance that allows studying the influence of the weak chiral Dzyaloshinskii–Moriya interaction on the physics of strongly correlated systems.

MnSi, as well as a number of other silicides and germanides of transition metals (FeSi, CoSi, FeGe, etc.), crystallizes into the structure type B20 (space group $P2_13$) [1]. This space group has no inversion center, which allows a helical (chiral) magnetic structure to exist in these compounds (which indeed have been revealed in MnSi, $Fe_{1-x}Co_xSi$, and FeGe).

We note that the specific features of the magnetic structure of these compounds significantly favored the development of adequate experimental and theoretical methods of neutron diffraction studies.

The magnetic phase transition temperature in MnSi (about 29 K at atmospheric pressure) decreases with increasing pressure and tends to zero at the pressure ≈ 1.4 GPa [2]. This circumstance, indicating the possibility of observing quantum critical phenomena, determined the subsequent interest in the investigations of MnSi at high pressures, which have revealed a number of intriguing features in the behavior of MnSi. A deviation from the Fermi-liquid behavior was discovered in the paramagnetic phase [3, 4]. An unusual spin state (partial order) was found in the

S M Stishov, A E Petrova Vereshchagin Institute for High Pressure Physics, Russian Academy of Sciences,
Kaluzhskoe shosse 14, 142190 Troitsk, Moscow region,
Russian Federation
E-mail: *sergei@hppi.troitsk.ru*

Received 28 February 2011, revised 6 April 2011
Uspekhi Fizicheskikh Nauk **181** (11) 1157 – 1170 (2011)
DOI: 10.3367/UFNr.0181.201111b.1157
Translated by S N Gorin; edited by A M Semikhatov

paramagnetic phase [5]. To explain these phenomena, new concepts were suggested, such as skyrmions [6] and a "helical spin crystal" [7] (also see [8]). Noteworthy is the interpretation of the results of small-angle neutron scattering (SANS) in the so-called A phase of MnSi in terms of a skyrmion crystal [9]. Here, we should keep in mind that the skyrmions in magnetic substances are vortex spin structures, which in some cases can 'crystallize' to form vortex lattices. The term 'skyrmion' is related to the name of the English physicist Tony Skyrme, who suggested a topological model of baryons (see [6] and the references in Appendix I).

The physical properties of MnSi have been under intense investigations for several decades at ambient and high pressures, which has led to a number of new results that are, in our opinion, of great importance for all of physics and, consequently, are of interest for a wide circle of readers of this journal.

It was initially planned that this review would be written together with S V Maleev and S V Grigor'ev (Konstantinov Institute of Nuclear Physics, St. Petersburg), who are the authors of a series of extensive studies on neutron scattering in MnSi. However, this did not happen and, in publishing this review, we expect that their review will also appear soon. For this reason, we virtually ignore some issues that require a qualified analysis of the results of neutron investigations. Nor do we consider some studies devoted to investigations using nuclear magnetic resonance and electron paramagnetic resonance methods or studies that do not lead to fundamentally new concepts.

Below, as the characteristics of the magnetic field, we use two quantities, the magnetic field strength H expressed in oersteds, and the magnetic induction B expressed in teslas ($1\ \mathrm{T} = 10^4$ Oe).

2. General characteristic of MnSi

MnSi is a weak itinerant-electron (band) ferromagnetic 3d metal that crystallizes into a B20-type noncentrosymmetric cubic structure characterized the space group $P2_13$ containing no inversion center. The primitive unit cell with the lattice parameter $a \approx 4.56$ Å contains four formula units.

The B20 structure type includes right-handed and left-handed enantiomorphic forms (Fig. 1). The coordinates of Mn and Si atoms of the right-hand form are:

$$(x,x,x,), \left(\frac{1}{2}+x,\frac{1}{2}-x,-x\right), \left(-x,\frac{1}{2}+x,\frac{1}{2}-x\right),$$
$$\left(\frac{1}{2}-x,-x,\frac{1}{2}+x\right),$$

where x takes the values $x_{\mathrm{Mn}} = 0.137$ and $x_{\mathrm{Si}} = 0.845$. The left-hand form corresponds to the replacement of x with $1 - x$ (see Fig. 1) [10, 11].

MnSi is a congruently melting compound and its single crystals can be obtained both by direct crystallization from the melt using Bridgman and Czochralski techniques, floating zone method, and so on, and by crystallization from the solution in the melt of some metals, e.g., tin. A magnetically ordered state in MnSi was discovered in [12], where it was also shown that the magnetic ordering in MnSi occurs at the temperature 30 K. In [13], a helical magnetic order was found in MnSi.

The magnetic structure of MnSi in a zero magnetic field can be described as a system of ferromagnetically ordered planes located parallel to the (111) crystallographic plane.

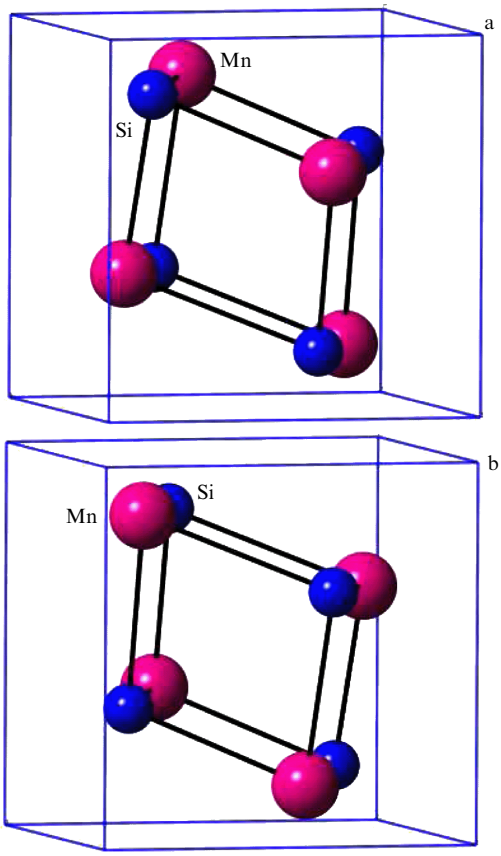

Figure 1. Crystal structure of (a) right-handed and (b) left-handed forms of MnSi.

The magnetic moment of each layer is turned by a small angle relative to the magnetic moment of adjacent layers due to the Dzyaloshinskii–Moriya interaction $D[\mathbf{S}_1 \times \mathbf{S}_2]$, which is nonzero in noncentrosymmetrical structures [14–16]. As a result, in the magnetically ordered phase (at temperatures less than ≈ 29 K), the spins form a left-handed incommensurate spiral with the wave vector ≈ 0.036 Å^{-1} (corresponding to the period 180 Å) in the [111] direction. We note that the relation between the structural and magnetic chirality has not so far been completely clarified [10, 11, 17].

The magnetic properties of MnSi are controlled by a hierarchy of three characteristic energies, including the isotropic exchange, the weak Dzyaloshinskii–Moriya interaction, and the even weaker anisotropic exchange, which successively determine the ferromagnetic ordering in the layers, the formation of the spiral (chiral) structure, and the direction of the wave vector of the spiral.

It is interesting to compare the properties of MnSi with the properties of the silicides of the nearest neighbors of Mn in the periodic system, i.e., Fe and Co. The FeSi and CoSi compounds, just as MnSi, crystallize into the B20 structure type. The lattice parameters in the MnSi–FeSi–CoSi row change quite weakly as the atomic radii of the metallic elements change (Table 1). The elastic properties of these compounds at low temperatures change monotonically in accordance with the variation of the lattice parameters (Table 2).

The lattice properties of MnSi, FeSi, and CoSi appear to depend on the number of electrons on the 3d shell of metallic elements quite weakly. However, the same circumstance has a dramatic effect on the electrical and magnetic properties of

Table 1. Lattice parameters a and chemical composition of helimagnets [18].

Compound*	a, Å	Atomic percent	
		Metal	Si
MnSi	4.5598(2)	50.63	49.37
FeSi	4.4827(1)	50.16	49.84
CoSi	4.444(1)	50.07	49.93
	4.4438(6)		

* The MnSi, FeSi, and CoSi compounds belong to the so-called berthollides, i.e., compounds of variable composition. The exact values of the lattice parameters and the chemical composition of these compounds depend on their history.

Table 2. Elastic constants C_{ij} of MnSi, FeSi, and CoSi [18] (Θ_D is the Debye temperature).

MnSi, $a = 4.5598$ Å, $\Theta_D = 660$ K			
C_{ij}	$T = 6.5$ K	$T = 78$ K	$T = 115$ K
C_{11}	3.2057	3.2045	3.2047
C_{44}	1.2615	1.2582	1.2540
C_{12}	0.8523	0.8574	0.8477
FeSi, $a = 4.483$ Å, $\Theta_D = 680$ K			
C_{ij}	$T = 6.5$ K	$T = 77.8$ K	$T = 292.8$ K
C_{11}	3.4626	3.4454	3.1670
C_{44}	1.3916	1.3858	1.2521
C_{12}	1.0576	1.0608	1.1298
CoSi, $a = 4.444$ Å, $\Theta_D = 625$ K			
C_{ij}	$T = 6.5$ K	$T = 77.8$ K	$T = 292.8$ K
C_{11}	3.5432	3.5404	3.4529
C_{44}	1.1847	1.1857	1.1593
C_{12}	1.3323	1.3331	1.3128

these compounds. Indeed, MnSi is a helical metallic magnet, FeSi is the so-called strongly correlated semiconductor with an unusual behavior of the magnetic susceptibility, and CoSi is a diamagnetic semimetal. The calculations of the energy band structures and density of states agree well with experimental data [19–21].

The magnetic moment of MnSi at $T = 1.4$ K calculated from the saturation magnetization in a magnetic field $H_c > 6.2$ kOe is $0.4\,\mu_B$ per Mn atom, whereas the approximation of the magnetic susceptibility in the paramagnetic phase by the Curie–Weiss relation yields the effective magnetic moment $2.2\,\mu_B$ per Mn atom [22]. Differences of this kind are considered to be a characteristic feature of band magnets.

Measurements of the thermal expansion and heat capacity of MnSi have demonstrated the existence of clearly pronounced anomalies in the vicinity of the magnetic phase transition, but did not lead to a definite conclusion on the nature of the phase transition [23]. The extrapolation of the C_p/T ratio to $T = 0$ gives an anomalously high value of the electronic heat capacity coefficient $\gamma \approx 36$ mJ mol^{-1} K^{-2}. The temperature dependence of the electrical resistivity at low temperatures is described well by a power law with an exponent close to 2, which indicates the Fermi-liquid behavior of the electron liquid in MnSi at ambient pressure. The electrical resistivity demonstrates a distinct anomaly in the region of the phase transition and tends to saturation at temperatures exceeding T_c [24, 25].

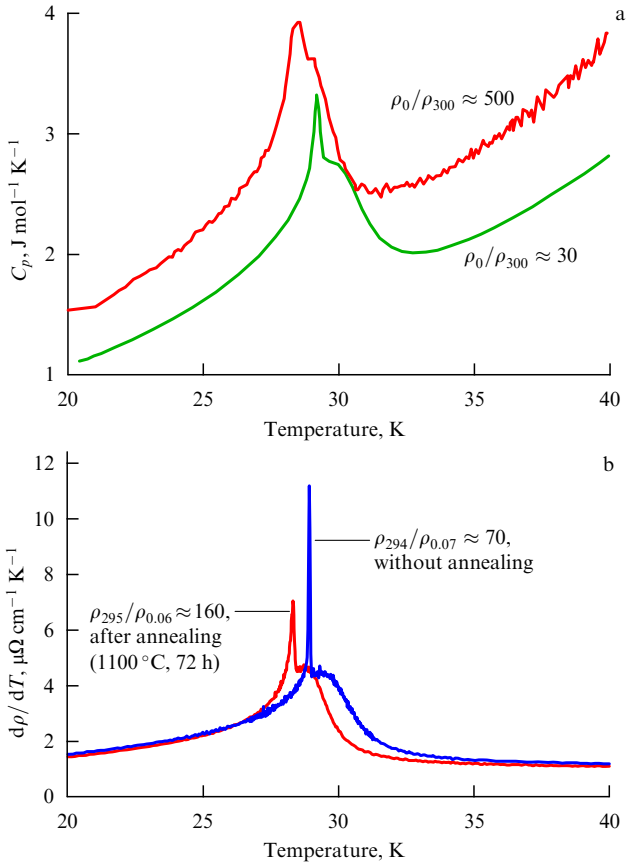

Figure 2. Effect of high-temperature annealing on (a) the heat capacity of MnSi (according to [26]) and (b) the temperature coefficient of resistivity of MnSi (V N Krasnorusskii and V N Narozhnyi, private communication).

In Sections 3 and 4, we describe new results of investigations of the physical properties of MnSi, which in some cases are based exclusively on our work performed on high-quality single crystals of MnSi.

Here, it is worth touching on the problem of the criterion of quality of crystals. In low-temperature investigations of metals, the magnitude of the ratio of the electrical resistivity at room temperature to the residual resistivity (at zero temperature) ρ_{295}/ρ_0 is usually chosen as such a criterion. We used just this criterion to estimate the quality of MnSi crystals. To increase ρ_{295}/ρ_0, crystals are frequently subjected to annealing for many hours at temperatures above 1000 °C. However, it turns out that this procedure adversely affects the characteristics of the phase transition (Fig. 2). Obviously, the ρ_{295}/ρ_0 criterion does not 'work' in the case of MnSi. On the other hand, the 'sharpness' of the phase transition can apparently serve as a qualitative indicator of the crystal perfection.

3. Physical properties of MnSi at ambient pressure

3.1 Magnetism

The most important characteristic of a magnetic substance is its response to an external magnetic field. The results of practically the first measurements have demonstrated an unusual behavior of the magnetic properties of MnSi (Figs 3, 4). The saturation magnetic moment of MnSi

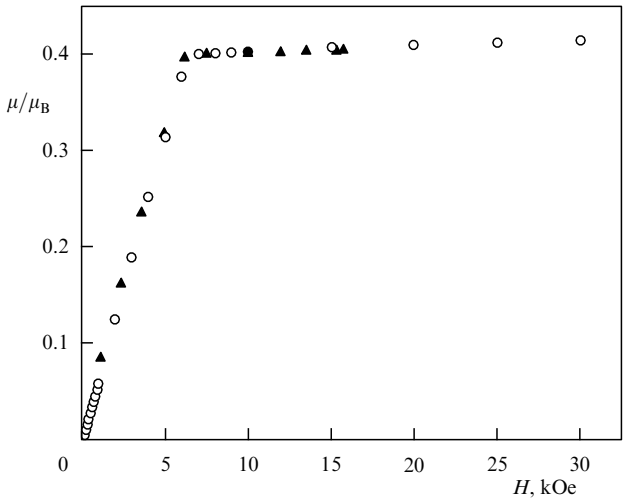

Figure 3. Saturation magnetic moment for MnSi: (▲) [22]; (○) [27].

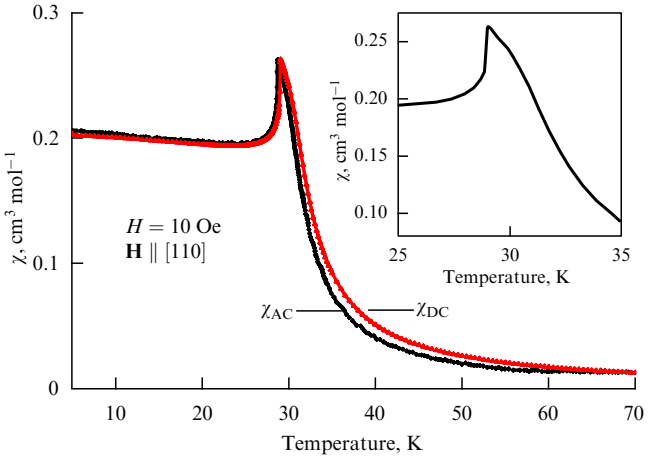

Figure 5. Magnetic susceptibility of MnSi in the vicinity of the phase transition [27] (χ_{AC} and χ_{DC} are the magnetic susceptibilities measured in an AC field and in a DC field).

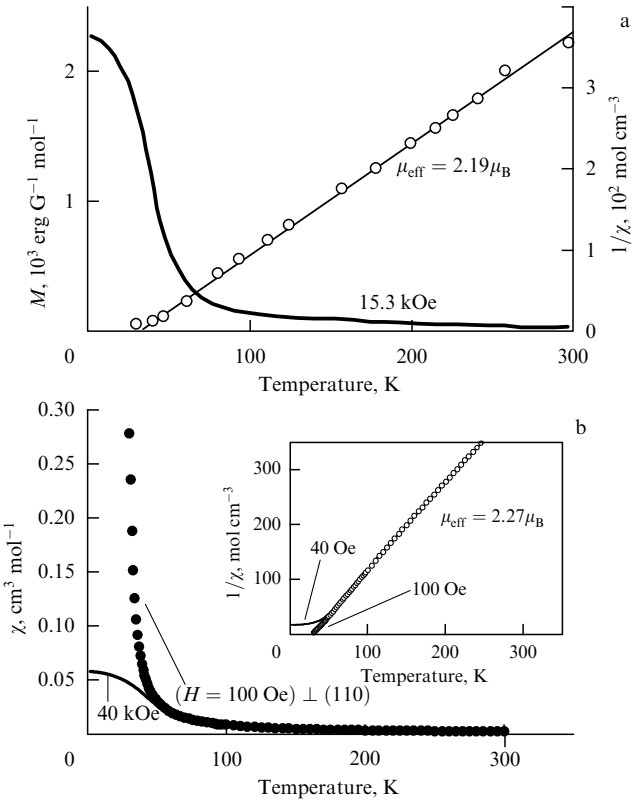

Figure 4. Magnetization and magnetic susceptibility of MnSi: (a) according to [22]; (b) according to [27] (the results corresponding to $H = 40$ kOe were obtained by J Thomson).

calculated from measurements in [22] was equal to 0.4 μ_B per Mn atom at $T = 1.4$ K. At the same time, the effective magnetic moment following from the Curie–Weiss behavior of the magnetic susceptibility of MnSi at $T > T_c$ is 2.19 μ_B per Mn atom. Later, this property of the magnetic characteristics of MnSi was assumed to be an intrinsic property of weak band magnets.

Figure 4b illustrates the results of recent measurements of the magnetic properties of MnSi obtained using a high-quality single crystal [27] in comparison with earlier data [22]. We note that the magnetization curves given in Fig. 4 were measured in the magnetic fields 15.3 and 40 kOe in the field of the induced ferromagnetic phase, and do not therefore contain any features indicating the existence of a phase transition (see the phase diagram in Fig. 6). Magnetic measurements in fields less than 6 kOe demonstrate a clearly pronounced anomaly in the magnetic susceptibility at $T \approx 29$ K, corresponding to the phase transition temperature (Fig. 5). In some studies, this feature of the magnetic susceptibility is called the λ anomaly, which, as a matter of fact, does not correspond to the reality. The shape of the anomaly shown in the inset in Fig. 5 can be regarded as a result of a jump-like increase in the magnetic susceptibility at the phase transition point. In the absence of such a jump, the magnetic susceptibility curve would look like the standard $\chi(T)$ dependence characteristic of a typical antiferromagnetic phase transition.

Figure 6 displays the magnetic phase diagram of MnSi according to the data in [28–30]. It follows from this diagram that the application of a magnetic field first transforms the helical spin structure into a conical structure and then orients all spins in one direction, forming a field-induced ferromagnetic phase.

It is noteworthy that in magnetic fields less than 4 kOe, the phase transition temperature only weakly depends on the field (see Fig. 6), which appears to indicate a finite magnitude of the order parameter. This fact speaks in favor of the interpretation of the magnetic phase transition in MnSi as a first-order phase transition. Some difference in the behavior of the phase boundary as a function of the magnetic field in Figs 6a and 6b does not change the essence of this conclusions.

Further investigations of the magnetic phase diagram of MnSi led to the discovery of the so-called A phase, which forms a 'pocket' in the $H-T$ region of stability of the helical phase (Fig. 6a). The physical nature of the A phase is the subject of an ongoing discussion, although solid evidence in favor of its skyrmion nature has appeared recently [9]. We return to the discussion of this question below (see Appendix I).

3.2 Heat capacity

The heat capacity of MnSi was measured in crystals of various perfection in a number of studies using different techniques [23, 26, 31]. The first measurements of the heat capacity of

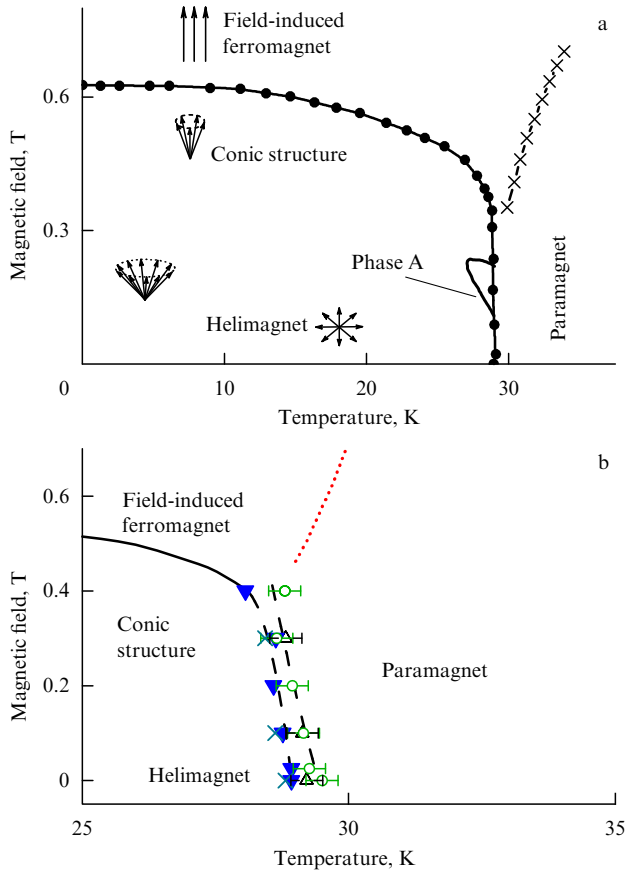

Figure 6. Magnetic phase diagram of MnSi: (a) according to ultrasonic investigations (● [28]) and the A phase according to [29]; (b) according to the measurements of thermal expansion (▼) and heat capacity (○) [30]. It is seen that in (b), in contrast to the data in [28] given in (a), the boundary between the helimagnetic and paramagnetic phases as a function of the magnetic field is tilted.

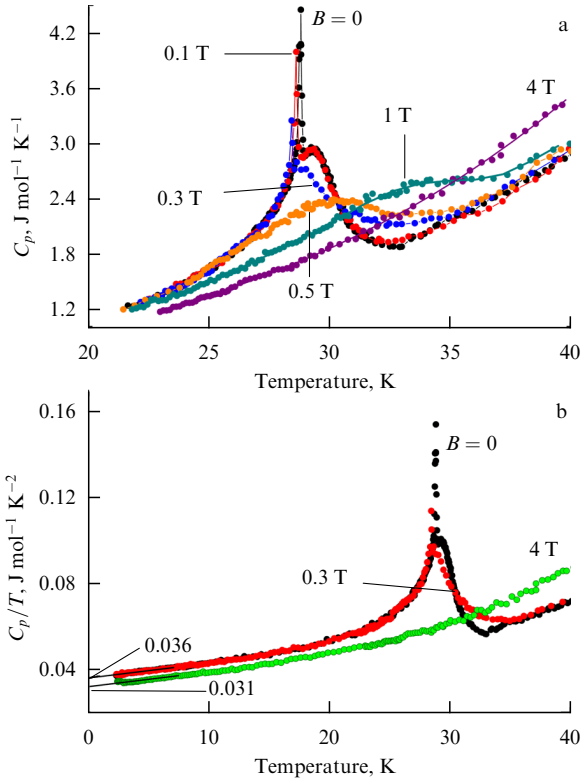

Figure 7. Heat capacity of MnSi in magnetic fields: (a) heat capacity in the phase transition region; (b) C_p/T ratio as a function of temperature.

MnSi were carried out (on samples of apparently moderate quality) in [23]. Nevertheless, by extrapolating the C_p/T ratio T to zero, Fawcett obtained a correct (according to the modern data) value of the electronic heat capacity coefficient $\gamma = 0.038$ J mol^{-1} K^{-2}. But an important feature (the sharp peak) in the heat capacity curve of MnSi in the phase transition region was not revealed. As a result, it was assumed in the physics community that the phase transition in MnSi should be regarded as a second-order transition in spite of the conclusions of the experimental and theoretical work [28, 29, 32].

New measurements of heat capacity were performed on high-quality crystals in magnetic fields up to 4 T (Fig. 7) [27, 30]. It can be seen that the temperature dependence of the heat capacity $C_p(T)$ at $B = 0$ is characterized by a sharp peak at $T \approx 28.8$ K, corresponding to the phase transition with a clearly pronounced 'shoulder' on its high-temperature side. An increase in the magnetic field to 0.3 T only insignificantly decreases the phase transition temperature and leaves the heat capacity of the magnetically ordered phase virtually unaffected, which apparently indicates a certain hardness of the magnetic structure and, consequently, a finite magnitude of the order parameter at the phase transition point in MnSi. The magnetic field 0.5 T transforms the system into a field-induced ferromagnetic state and eliminates the phase transition (see Fig. 6).

Figure 7b, which illustrates the behavior of the C_p/T ratio, allows determining the electron heat capacity coefficients as $\gamma = 36$ mJ mol^{-1} K^{-2} at $B = 0$ and $\gamma = 31$ mJ mol^{-1} K^{-2} at $B = 4$ T. The value of γ at $B = 0$ agrees well with the earlier estimate (in which the evident error in the order of magnitude was corrected) [23]. The high value of γ indicates a significant effective electron mass in MnSi. A rough estimate performed in [30] gives $m^*/m \approx 36$.

The obtained value of γ was used in [33] in the analysis of the behavior of the magnetic contribution to the heat capacity of MnSi, which revealed the existence of negative contributions to the heat capacity and entropy at $T > T_c$ (see Appendix II for the details).

To conclude this section, we note that both experimental and calculated data are currently available that allow reliably determining the phonon contribution to the heat capacity of MnSi (see [33] and Appendix II). Nevertheless, a complete analysis of the behavior of the heat capacity of MnSi, including the separation of the magnon contribution, is difficult in view of the existence of a large anomaly in the phase transition region. This anomaly cannot be described in terms of the standard models of phase transitions; its description requires a nontrivial approach. We also note that the data obtained in [34, 35] indicate the existence in MnSi of helical magnons with a specific dispersion law.

3.3 Thermal expansion

The heat expansion of MnSi was first measured in [23], where a wide negative anomaly of the thermal expansion coefficient was revealed in the vicinity of the phase transition. A complex structure of the anomaly was observed (apparently, also for the first time) in [36]. The anomaly (noted previously in the example of heat capacity) was characterized, apart from the

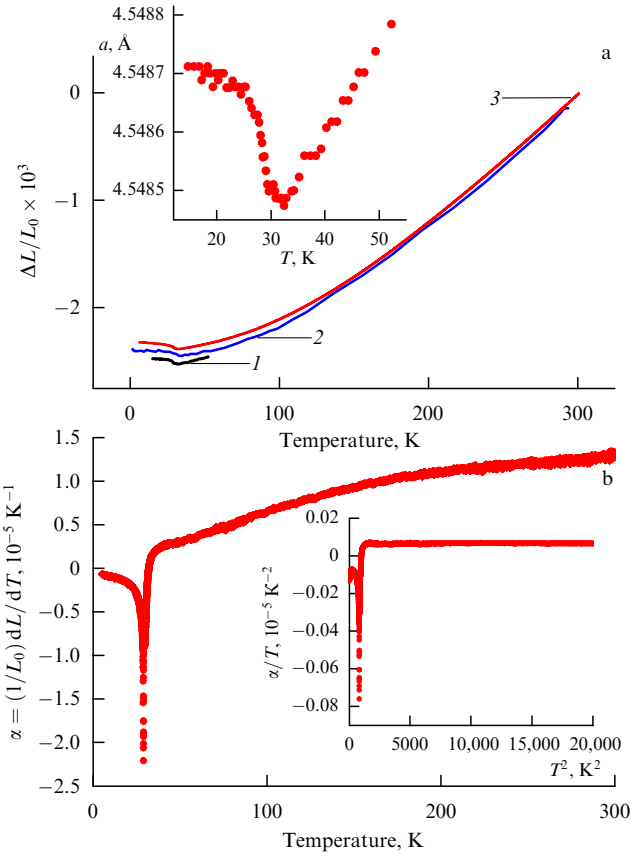

Figure 8. Thermal expansion of MnSi [27, 30]: (a) linear thermal expansion according to (*1*) XRD data, (*2*) neutron-diffraction data, and (*3*) dilatometric data; (b) thermal-expansion coefficient (the inset illustrates the linear behavior of the TEC).

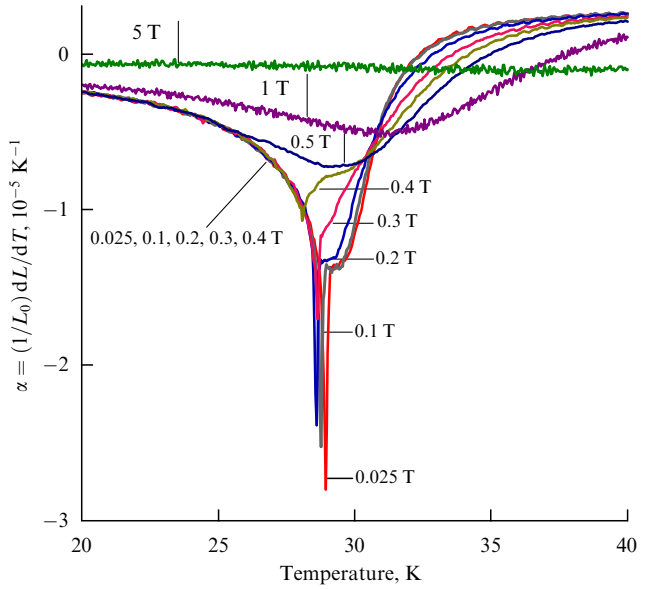

Figure 9. Thermal expansion coefficient of MnSi in the vicinity of the phase transition [27].

main negative peak at the phase transition point, by a side minimum (shoulder) at a temperature approximately 2 K above T_c.

Detailed investigations of the thermal expansion of MnSi have been performed in [27, 30]; the results are given in Figs 8 and 9.

Figure 8a shows the behavior of the linear thermal expansion coefficient of MnSi according to the data obtained using capacitance dilatometry and X-ray and neutron diffraction. All the results are qualitatively consistent, although from the quantitative standpoint, preference should be given to the X-ray diffraction data. On the other hand, data on the behavior of the thermal expansion coefficient are mainly based on the results of dilatometric measurements, because neither X-ray nor neutron diffraction have sufficient resolution for the investigation of the fine details of thermal expansion of MnSi in the vicinity of the phase transition.

Figure 8b displays the temperature dependence of the linear thermal expansion coefficient $\alpha = (1/L_0)\,dL/dT$ of MnSi. It can be seen that the behavior of α in the temperature range 0–35 K is determined by magnetostrictive and fluctuation effects arising as a result of ordering of magnetic moments. The representation of the results as a dependence of α/T on T^2 does not reveal a noticeable lattice contribution to the thermal expansion of MnSi but shows a linear increase in the thermal expansion coefficient α in the temperature range 35–150 K (see the inset in Fig. 8b).

Figure 9 illustrates the effect of a magnetic field on the thermal expansion coefficient of MnSi. Again, as in the case of heat capacity, a moderate magnetic field (up to 0.4 T) leaves the thermal expansion of the helical phase virtually unaffected but substantially influences the behavior of the paramagnetic phase. We note that the side minimum (shoulder) vanishes faster than the main minimum corresponding to the phase transition. In any case, the behavior of the thermal expansion coefficient of MnSi confirms the earlier conclusion of a finite value of the order parameter at the phase transition point, which obviously contradicts the concept of its continuity. We also note that the fast degradation of the phase transition in magnetic fields between 0.4 and 0.5 T indicates the formation of a field-induced ferromagnetic spin structure in MnSi.

3.4 Elastic properties and ultrasound attenuation

In our previous work [37], we studied the elastic properties of MnSi and attenuation of ultrasound in it using the digital pulsed technique of measurements [38]. The results in [37] are presented graphically in Fig. 10 (selected numerical data are given in Table 2). As can be seen from Fig. 10a, the magnetic phase transition in MnSi is accompanied by a profound anomaly (softening) of elastic moduli and of their combinations that determine the propagation of longitudinal ultrasonic waves. At the same time, the magnetic phase transition manifests itself as a small change (jump) in the elastic moduli, which is localized on the low-temperature side of the anomalies. We note that both these features excellently correlate with the behavior of the heat capacity, the thermal expansion coefficient, and the thermal resistivity coefficient (see Section 3.5), except that the sharp maxima and minima of these thermodynamic and transport properties at the phase transition point are replaced by moderate jumps of the elastic moduli. It is precisely such a behavior of the elastic moduli that should be expected in the case of a weak first-order phase transition [37].

In contrast to the 'longitudinal' moduli, the shear moduli change insignificantly, mainly following the variation of the volume deformation arising upon magnetic ordering

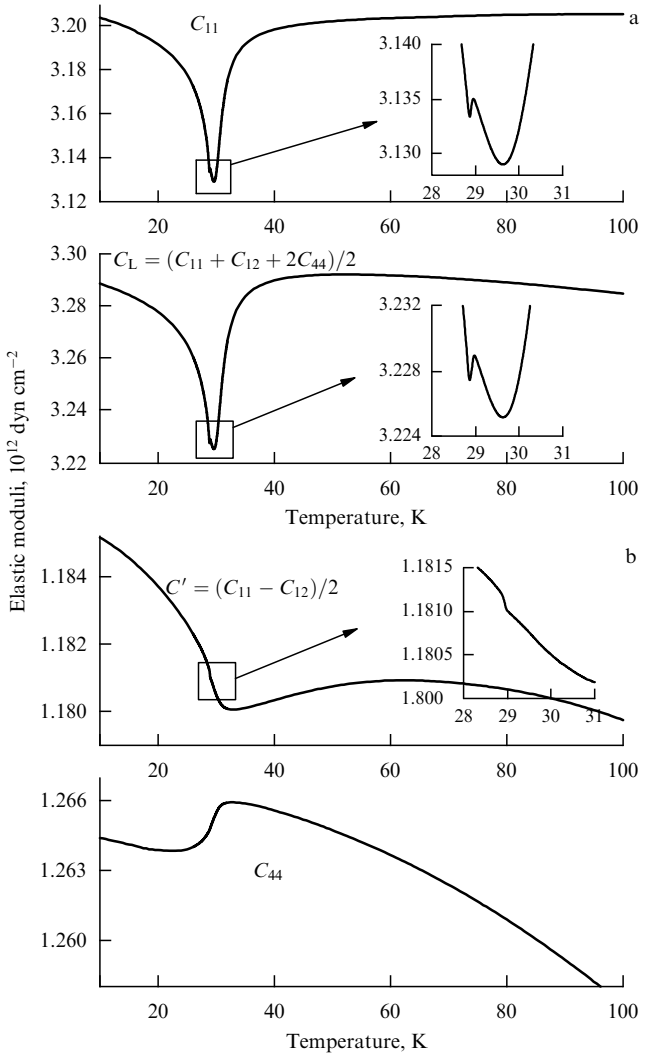

Figure 10. Variation of the elastic moduli during the phase transition in MnSi [37].

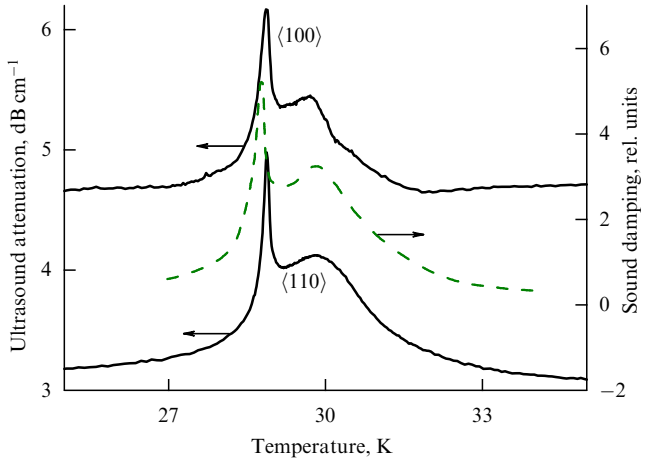

Figure 11. Ultrasound attenuation during the phase transition in MnSi: solid curves, data in [37]; dashed curve, data in [39].

(Fig. 10b). This significant difference in the behavior of the longitudinal and transverse elastic characteristics appears to be related to the insignificant role of the interaction between the ionic and electronic subsystems during the magnetic phase transition in MnSi, simultaneously emphasizing the itinerant-electron nature of magnetism in this substance.

We now turn to Fig. 11, which illustrates the attenuation of ultrasound waves. It is interesting that the total structure of the attenuation curves (the main peak and the side maximum) represents an almost exact copy of the corresponding curves that characterize the behavior of the heat capacity, the thermal expansion coefficient (with the inverse sign), and the thermal resistivity coefficients (see Section 3.5). It is noted in [37] that the main peak in the attenuation curves appears to be due to the adiabaticity distortion caused by a finite change in the entropy under the first-order phase transition in MnSi.

The investigations in [37] also reveal a very important fact, which clearly demonstrates that the magnetic phase transition at $T = 28.8$ K in MnSi is only one of the features of a global transformation accompanied by the appearance of anomalies of physical quantities with extrema located at temperatures somewhat higher than the phase transition temperature. The nature of this transformation is still not completely clear.

3.5 Electrical resistivity

In this section, we only touch on the temperature behavior of the electrical resistivity of MnSi in the vicinity of the phase transition at ambient pressure according to [27]. As we can see from Fig. 12c, the resistivity of MnSi increases monotonically, demonstrating a tendency to saturation at temperatures above T_c. Just at the phase transition point, a small ($\approx 1.6\%$), slightly smeared jump is observed. The derivative $d\rho/dT$ exhibits a wide maximum with a sharp peak, which is associated with a smeared δ function. It is instructive to compare the overall shape of the $d\rho/dT$ function with the corresponding curves characterizing the behavior of heat capacity and thermal expansion (see Fig. 12).

3.6 Nature of the phase transition in MnSi

The order parameter in MnSi is the spin density (slowly changing in space) $\mathbf{S}(\mathbf{r}) = \mathbf{S}_1 \cos(\mathbf{qr}) - \mathbf{S}_2 \sin(\mathbf{qr})$, where $\mathbf{S}_1 \perp \mathbf{S}_2$ and $\mathbf{q}$ is the wave vector of the spiral. The expansion of the free energy of MnSi in powers of the spin density does not contain odd terms because of the symmetry under time reversal, which implies the possibility of the realization of the magnetic phase transition in MnSi as a second-order phase transition [32, 40]. Nevertheless, the renormalization-group analysis performed in [32] led the authors of [32] to the conclusion of the jump-like nature of the phase transition in MnSi induced by fluctuations. At that time, this conclusion was supported by the experimental data obtained in investigations of the magnetic phase diagram of MnSi [28, 29].

The modern data generalized in Fig. 12 demonstrate sharp peaks in the heat capacity curves, the thermal expansion coefficient, and the thermal resistivity coefficient, and slightly smeared jumps in the corresponding integrated curves, which allows interpreting the phase transition in MnSi as a weak first-order phase transition. Ultrasonic investigations, which revealed jumps in a number of elastic constants at the phase-transition point, agree well with this statement (Fig. 10a).

On the whole, however, the situation is by no means so simple: as we can see from Figs 11 and 12, in the curves that characterize the behavior of the heat capacity, the thermal expansion coefficient, the thermal resistivity coefficient, and ultrasound attenuation during the phase transition in MnSi, besides a sharp peak corresponding to the first-order phase

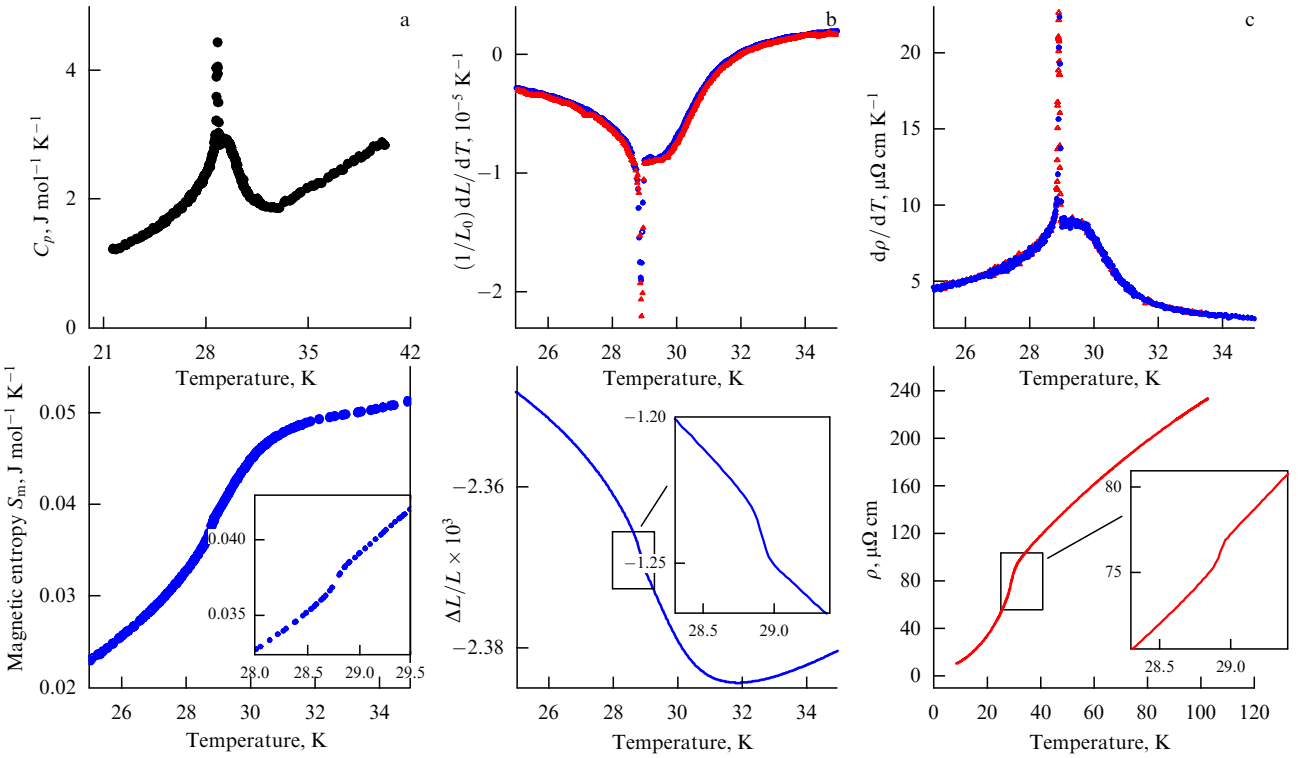

Figure 12. Behavior of thermodynamic quantities and the electrical resistivity during the phase transition in MnSi (according to [3, 27]). For clarity, in the inset given in (b), the background component has been subtracted from the total curve.

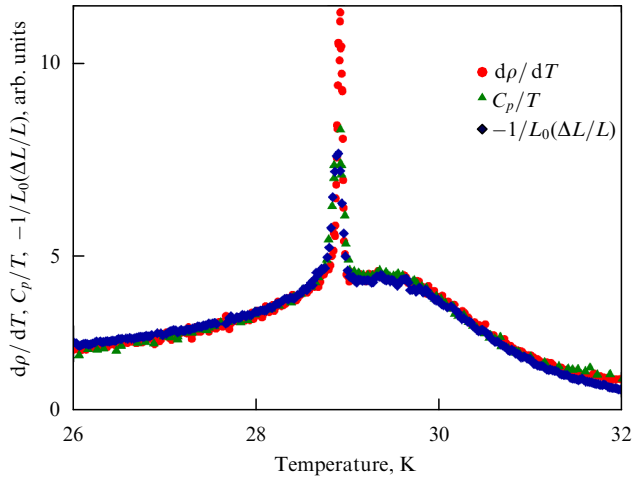

Figure 13. Reduced values of the heat capacity, the thermal expansion coefficient, and the thermal resistivity coefficient of MnSi in the vicinity of the phase transition [3].

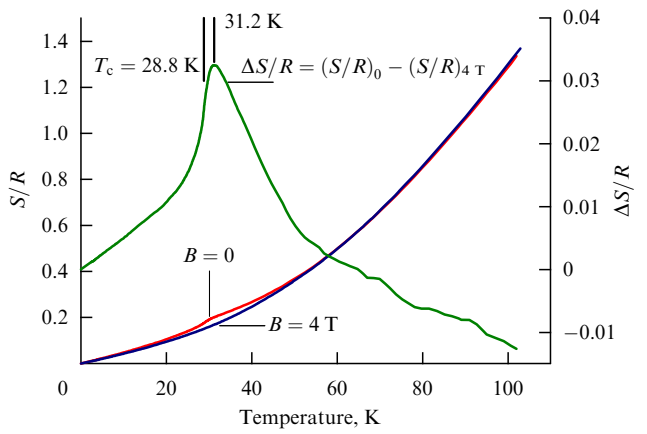

Figure 14. Entropy of MnSi calculated from the data on heat capacity measured at $B = 0$ and $B = 4$ T [30, 33]. The differential curve $\Delta S/R$ demonstrates that the drop in the entropy occurs at temperatures somewhat higher than the phase transition temperature.

transition, there also exist flat maxima or a minimum of the thermal expansion coefficient. It is surprising that the behavior of the above-mentioned quantities in the vicinity of the phase transition can be represented in the form of a single reduced curve (Fig. 13); still, this does not explain the nature of the flat extrema mentioned above.

Useful information can be obtained from Fig. 14, which demonstrates that a significant decrease in the entropy occurs beginning from a temperature of 31.2 K, close to the temperature of the corresponding extrema. In this connection, it is noteworthy to recall the ideas on the possible splitting of the phase transition in chiral magnetic systems into two transitions, magnetic and chiral, separated by a certain temperature interval [41, 42]. Papers [6, 43] should also be mentioned, in which the effects observed at $T > T_c$ are ascribed to the formation of skyrmions.

4. Phase diagram and investigations of MnSi at high pressures

4.1 Phase diagram

The first experiments on the effect of high pressure on the magnetic phase transition temperature T_c in MnSi were described in [3]. It was found that T_c decreases as the pressure increases, tending to zero at the pressure

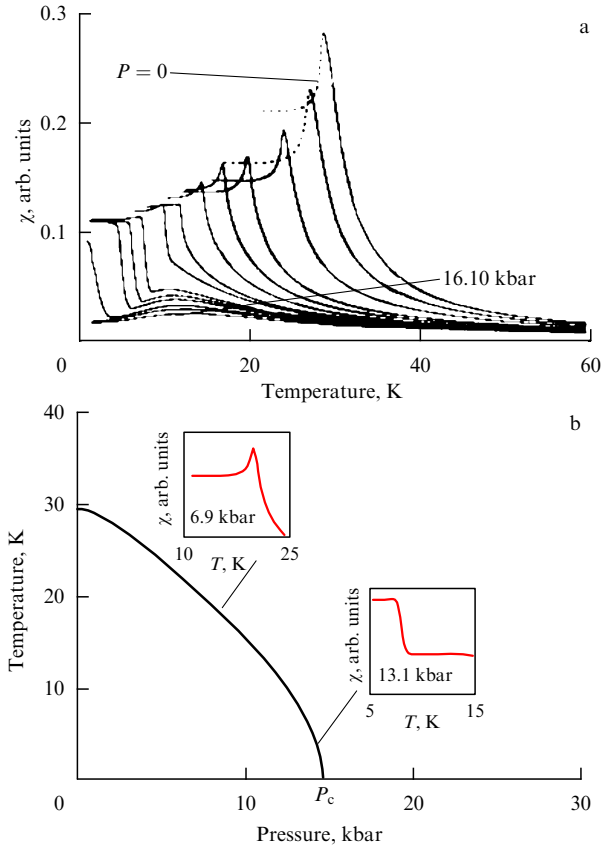

Figure 15. (a) Magnetic susceptibility and (b) phase diagram of MnSi according to [44, 45].

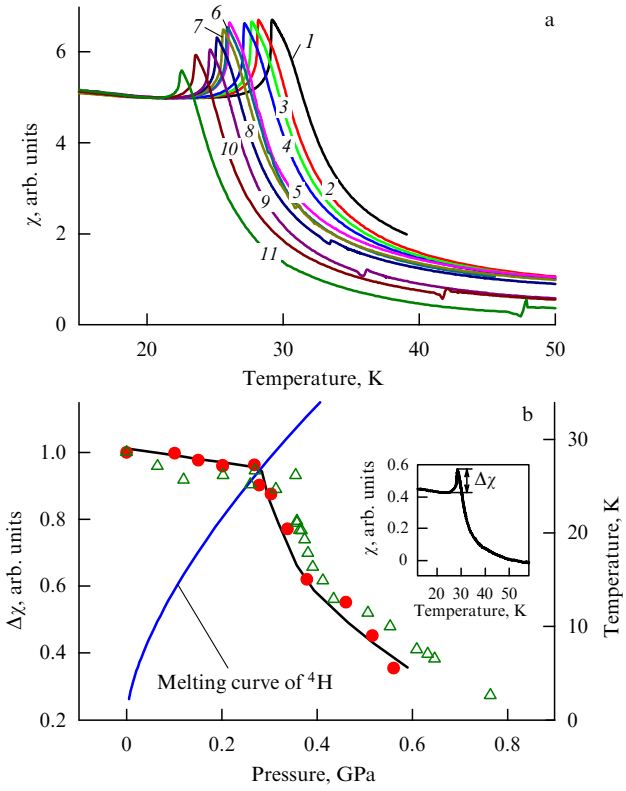

Figure 16. (a) Temperature dependence of the magnetic susceptibility and (b) pressure dependence of the peak of the magnetic susceptibility of MnSi according to [50]. Curves *1–11* in (a) respectively correspond to the pressures 0, 0.1, 0.15, 0.201, 0.268, 0.278, 0.303, 0.338, 0.379, 0.460, and 0.561 GPa. The symbols ● and △ in (b) correspond to two different series of measurements. The height of the peak of the magnetic susceptibility can be seen to decrease sharply with the solidification of helium, which serves as the pressure-transmitting medium.

≈ 1.4 GPa, which suggested the possibility of observing quantum critical phenomena in MnSi.

Later, numerous studies appeared that confirmed this observation [24, 44–48]. One such study, [44], has played a special role in the subsequent investigations of MnSi (also see [45]). Based on measurements of the magnetic susceptibility, it was stated in [44] that a tricritical point with coordinates ≈ 12 K and ≈ 1.2 GPa exists on the phase transition line in MnSi. This conclusion was based on experimentally observed changes in the evolution of the magnetic susceptibility of MnSi in the vicinity of the phase transition [44, 45] with changing pressure (Fig. 15). The authors assumed that the degeneracy of the peak of magnetic susceptibility indicates a change in the order of the phase transition. A theory developed later stated the inevitability of a discontinuous character of the ferromagnetic phase transition at low temperatures [49].

New investigations of the magnetic phase diagram of MnSi, whose important feature was the use of helium as the pressure-transmitting medium, were performed in [50]. The results of these studies have demonstrated clearly (Fig. 16) that the magnetic susceptibility of MnSi is quite sensitive to nonhydrostatic stresses, which arise even in solid helium, and that the shape of the $\chi_{AC}(T)$ dependence cannot be used to decide on the character of the phase transition. On the other hand, the results of the investigations of the behavior of the MnSi resistivity and its temperature derivative $d\rho/dT$ in the vicinity of the phase transition at high pressures do not indicate a change in the character of the phase transition (Fig. 17). Therefore, taking the data given in Section 3.6 into account, we can assume that the magnetic phase transition in MnSi is a first-order phase transition in the entire range of the existence of the magnetic phase. Nonetheless, the behavior of the temperature derivative $d\rho/dT$ can hardly be interpreted unambiguously. As can be seen from Fig. 17a, the sharp peak of $d\rho/dT$ corresponding to the magnetic phase transition is broadened as the pressure increases, whereas the width of the anomaly (still of an unclear origin), which accompanies the phase transition, tends to zero (Fig. 17b). The last conclusion agrees with the results of measurements of the thermal expansion of MnSi [51]. We emphasize that the sharp peak in $\alpha(T)$ curves (see Figs 8, 9) cannot be resolved experimentally [51] because of the limitations of the method.

The behavior of the linear thermal expansion of MnSi $\Delta L/L$ in a wide range of pressures is shown in Fig. 18. It can be seen that the interval ΔT of the broad anomaly $\Delta L/L$ narrows strongly with increasing pressure, which gives the impression of a jump-like change in the volume ($\Delta L/L \sim 10^{-5}$) in MnSi with the phase transition at $T \to 0$ (Fig. 19). But the behavior of the extremely small volume jump ($\Delta L/L \sim 10^{-6}$) observed at atmospheric pressure remains unclear.

Returning to Fig. 17a, we note that the sharp peak and the broad anomaly appear to merge into a common maximum, leading, in the integral representation, to the picture shown in Figs 18 and 19. Nevertheless, the total situation is quite ambiguous and requires additional investigation.

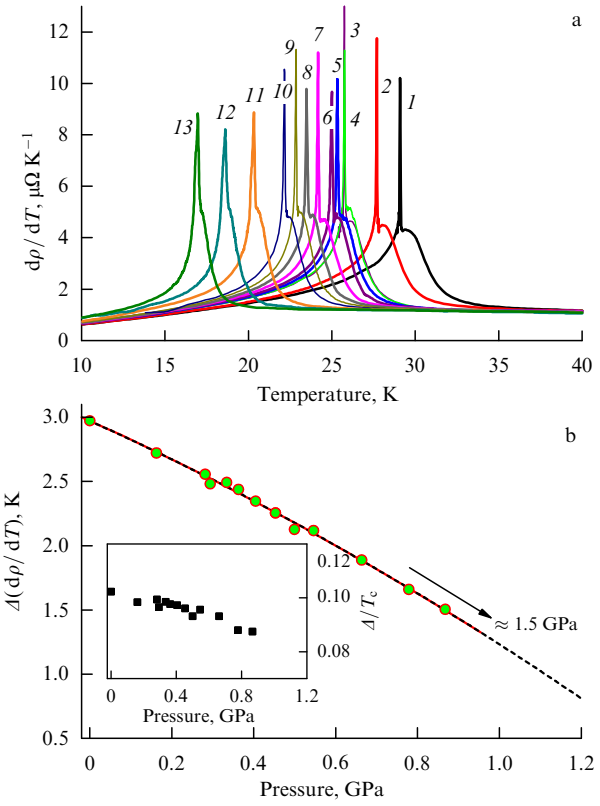

Figure 17. (a) Temperature dependence of the thermal resistivity coefficient $d\rho/dT$ of MnSi on T at different pressures in the region of the phase transition. (b) Pressure dependence of the width of the corresponding peaks $\Delta(d\rho/dT)$ measured at $d\rho/dT = 3$ μΩ cm K^{-1} [50]. Curves *1–13* in (a) correspond to the respective pressures 0, 0.163, 0.281, 0.294, 0.334, 0.363, 0.405, 0.453, 0.5, 0.55, 0.664, 0.779, and 0.868 GPa. The inset in (b) shows the pressure dependence of the ratio of the peak width to the phase transition temperature. The peak width is extrapolated to zero at the pressure corresponding to the quantum phase transition in MnSi at $T = 0$.

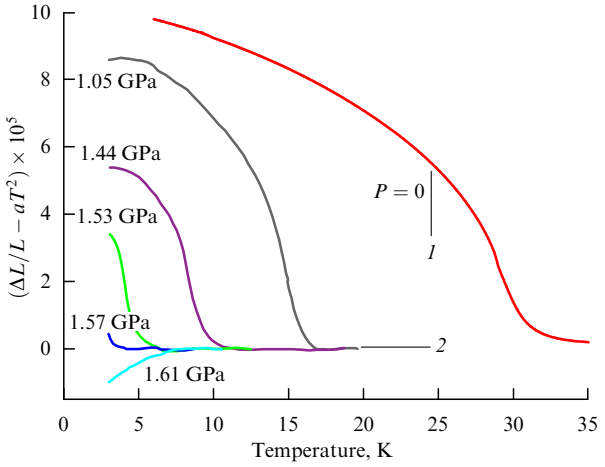

Figure 18. Thermal expansion of MnSi after the subtraction of the background component (aT^2) at various pressures: (*1*) according to [30]; (2) data from [51].

4.2 Non-Fermi-liquid behavior

The results mentioned in Section 4.1 appear to indicate that the quantum phase transition in MnSi at $T \to 0$ is a first-order phase transition, which generally excludes the development of quantum critical phenomena and related effects, such as a non-Fermi-liquid behavior of the resistivity and a logarithmic divergence of the heat capacity.

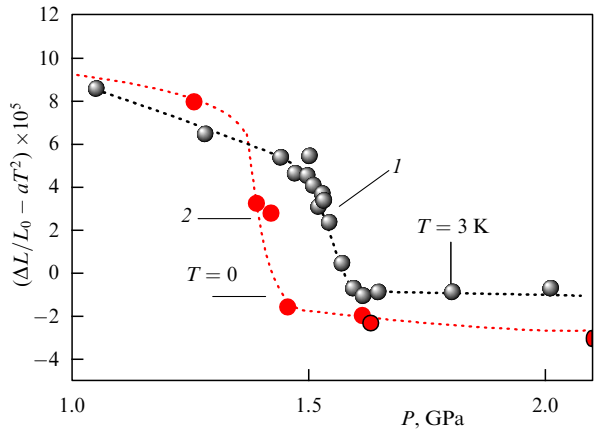

Figure 19. Relative variations of (*1*) the length of an MnSi sample [51] and (*2*) the lattice parameter of MnSi [52] at low temperatures and high pressures.

As was shown in [3, 4], the resistivity of MnSi in the paramagnetic phase at $P > P_c$ (≈ 15 kbar) and $T < 5$ K is described by a power law $\Delta\rho \propto T^n$ with the exponent $n = 1.5$ (we recall that $n = 2$ for the Fermi liquid and $n = 1$ in the quantum critical region) (Fig. 12). It is surprising that the region of the non-Fermi-liquid behavior extends at least to the pressure of 48 kbar ($\approx 3P_c$). With a further increase in pressure, the exponent n increases to 1.7 [53].

However, the data in [53] should be considered with a certain amount of skepticism, because the conditions of the corresponding measurements can hardly be called hydrostatic. Nevertheless, the very fact of the non-Fermi-liquid behavior of the temperature dependence of the resistivity of MnSi in a significant range of pressures $P > P_c$ is beyond dispute (Fig. 20).

The character of the manifestations of the non-Fermi-liquid behavior in MnSi suggests that it can have no relation to the quantum criticality, which poses a question on the origin of this phenomenon. In this connection, we should keep in mind that the $\sim T^{3/2}$ dependence of the electrical resistivity has been found in many amorphous metals and spin glasses [54]. The theory of resistivity of MnSi with the scattering of electrons on skyrmions taken into account to explain the $T^{3/2}$ law was suggested in [55] (for skyrmions, see Appendix I).

4.3 'Partial' helical order in the non-Fermi-liquid phase of MnSi

Figure 21 presents the results of small-angle neutron scattering (SANS) investigations of the magnetic superstructure in MnSi at ambient and high pressures according to [5]. It follows from this figure that the Bragg reflections with the wave vector **q** ($q = 0.037$ Å^{-1}) directed along [111], which characterize the magnetic spiral at ambient pressure, do not disappear completely in the region of the non-Fermi-liquid paramagnetic phase. The measurements at $P > P_c$ and $T < T_0$ (Fig. 21) reveal the existence of reflections corresponding to the magnetic spiral with the wave vector **q** ($q \approx 0.043$ Å^{-1}) continuously distributed over the angular space, with a maximum in the [110] direction. According to [5], the magnetic phase transition at P_c is therefore a reorientation phase transition and is determined by the

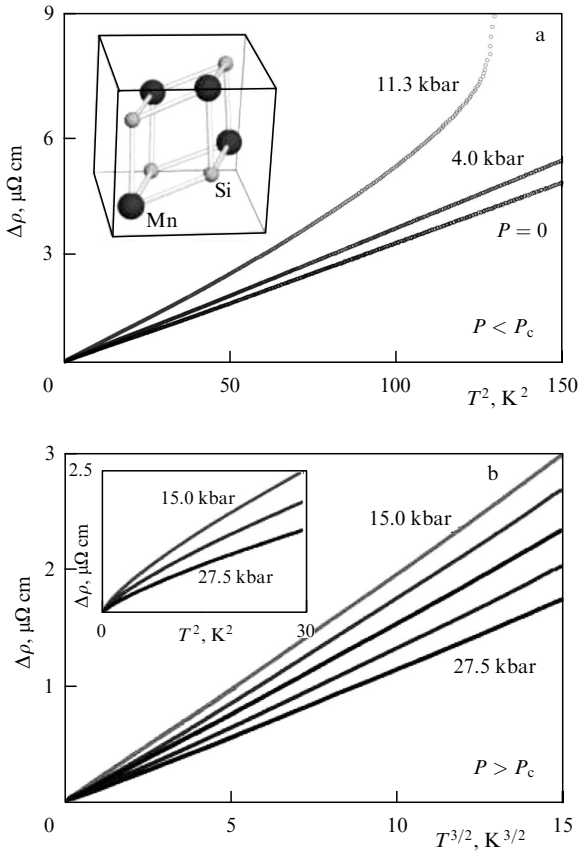

Figure 20. Electrical resistivity of MnSi as a function of temperature at high pressures [4] ($\Delta\rho = \rho - \rho_{T=0}$; P_c is the pressure of the quantum phase transition at $T = 0$).

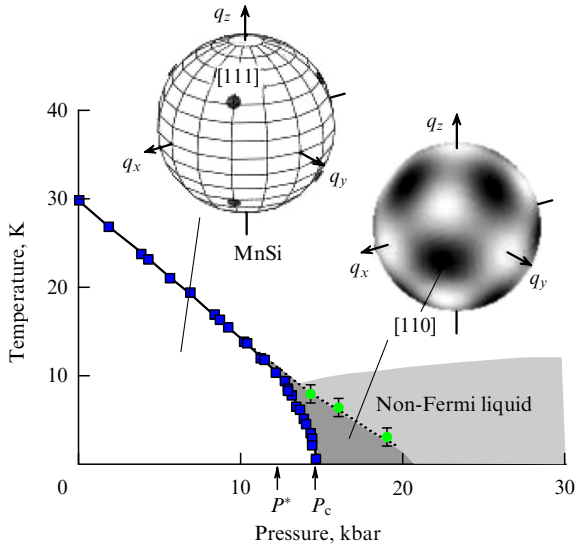

Figure 21. Small-angle neutron scattering in MnSi at ambient and high pressures (schematic) [5]. Square symbols correspond to the magnetic phase transition temperature; circles correspond to the temperature of the crossover between the paramagnetic phase and the state of partial ordering; P^* is the pressure corresponding to a hypothetical tricritical point; P_c is the pressure of the magnetic phase transition at P^*.

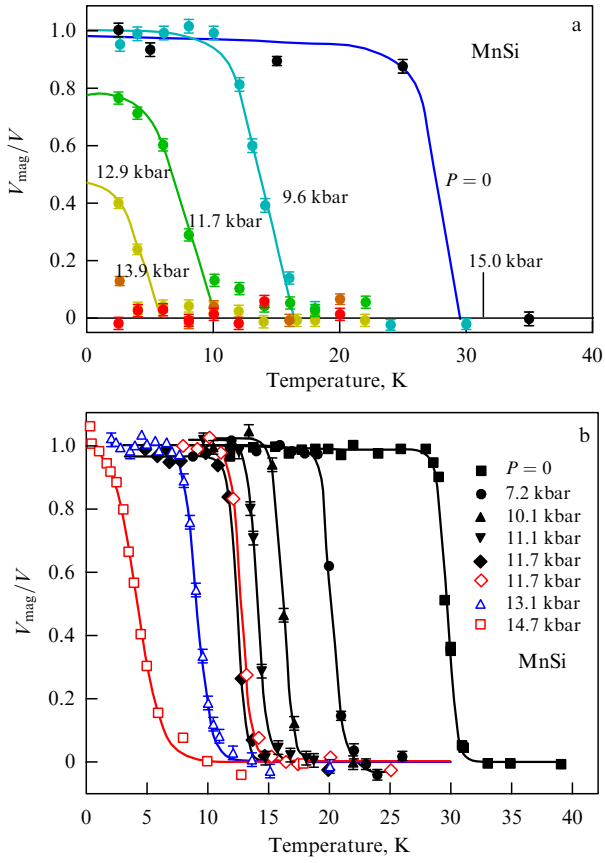

Figure 22. Magnetic volume fraction V_{mag}/V in MnSi as a function of temperature at high pressures: (a) data from [56] and (b) data from [58].

smallest of the three characteristic energies (see Section 2) responsible for the direction of the magnetic spiral in MnSi.

On the other hand, we warn readers against a noncritical perception of the above results. The use of fluorinert as a pressure-transmitting medium in neutron-diffraction investigations at high pressures is not optimal from the standpoint of conditions of hydrostaticity and sometimes leads to wrong conclusions.

4.4 Phase separation in MnSi at high pressures

The phase separation observed in a number of magnetic systems is by no means a universal indicator of a first-order phase transition, whereas such a transition is necessarily accompanied by phase separation.

In this connection, it is interesting to investigate the phase separation in MnSi at high pressures using muon spin spectroscopy (μSR) [56, 58]. It has been stated that the content of the magnetic fraction decreases rapidly starting with a pressure of 11.7 kbar, which means the existence of a phase separation outside the first-order phase transition region (Fig. 22a). This fact was given special importance, which we do not fully appreciate [56]. The phase inhomogeneity in MnSi at high pressures was also noted in [57].

However, new μSR investigations of MnSi [58] indicate an almost 100% amount of the magnetic fraction at pressures up to the value corresponding to the phase transition (Fig. 22b). The origin of the contradiction appears to lie in the violation of the hydrostaticity condition in investigations at high pressures (see the discussion in [58]).

5. Conclusions

To summarize, two problems that require special attention should be noted, in our opinion.

(1) As is emphasized in this review, the heat capacity, the thermal expansion coefficient, the thermal resistivity coefficient, elastic moduli, and the ultrasound attenuation coefficient during the phase transition in MnSi exhibit flat maxima (or a minimum in the case of the thermal expansion coefficient) at a temperature that is somewhat higher than T_c (see Section 3). In some cases, this feature is so strongly pronounced (see, e.g., the behavior of elastic moduli in Fig. 10) as to suggest the occurrence of some global transformation in the spin subsystem of MnSi, whose nature is yet to be clarified. In view of this impressive feature, the phase transition at $T \approx 29$ K seems only an insignificant event. This situation is excellently illustrated by the behavior of the entropy (see Fig. 14).

The clarification of the nature of this transformation and of its interrelation with the phase transition appears to be one of the primary problems to be solved.

(2) It follows from the results of measurements of thermal expansion of MnSi at high pressures (see Fig. 18) that the wide large anomaly corresponding to the flat minimum of the thermal expansion coefficient narrows strongly as the pressure increases, which possibly suggests a jump-like volume change in MnSi in the phase transition in the limit as $T \to 0$. This observation agrees with the data in Fig. 17, where the sharp peak of $d\rho/dT$ corresponding to the magnetic phase transition is broadened with increasing pressure, whereas the width of the flat anomaly of unclear origin, which accompanies the phase transition, tends to zero (Fig. 17b). Apparently, the sharp peak and the wide anomaly merge into a common maximum, producing a kind of a quantum tricritical point, as is shown in the hypothetical phase diagram in Fig. 23.

The vicinity of the quantum phase transition in MnSi at the pressure $P_c \approx 15$ kbar is therefore a kind of 'treasure island,' whose map is fully packed with labels for 'skyrmions,' 'partial spin order,' 'non-Fermi-liquid phase,' and 'quantum tricritical point.' However, no complete certainty exists that the labels are located correctly or that their names correspond to reality. It is also unclear whether there exist paths that connect these labels to a common system.

Therefore, detailed investigations of the phase diagram of MnSi at high pressures and low temperatures under truly hydrostatic conditions seem to be a necessary step in solving the above problems. However, such experiments seem to be hardly feasible at present in view of the extremely high sensitivity of MnSi to nonhydrostatic stresses. New approaches should be developed in the field of low-temperature techniques of high pressures.

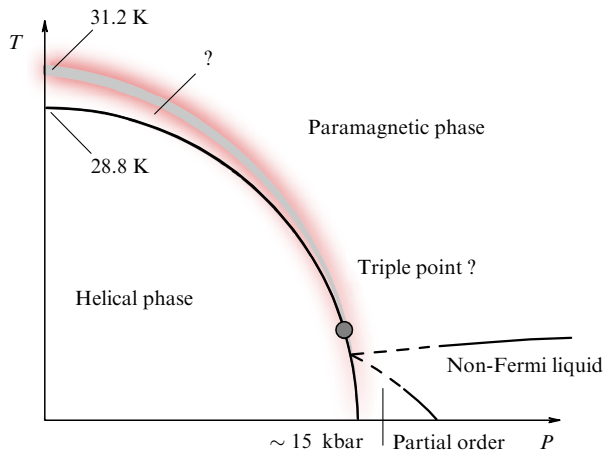

Figure 23. Hypothetical phase diagram of MnSi.

6. Appendices

Appendix I: Nature of the A phase and skyrmions

The wave vector of the magnetic spiral in MnSi in a zero magnetic field is known to be oriented in the direction of the spatial diagonal of the cubic unit cell [111]. At $T < T_c$, four domains are formed in MnSi, corresponding to four equivalent [111] directions. At low temperatures, the application of a magnetic field $B \approx 0.1$ T leads to the monodomainization of the sample, which acquires a conic magnetic structure and eventually passes into a field-induced ferromagnetic state at $B \approx 0.6$ T [28]. A somewhat different situation arises at temperatures close to T_c. In this case, as was established by the investigations of ultrasound, magnetization, and so on [29], a so-called A phase exists in magnetic fields $\approx 0.120-0.200$ T at temperatures from T_c to ≈ 27 K, whose spin structure is still the subject of debate. Initially, it the A phase was assumed to be paramagnetic [29], but experiments on neutron scattering revealed the existence of a magnetic order [59, 60].

The first ideas concerning the magnetic structure of the A phase, which were based on neutron-diffraction studies, amounted to the assumption that the wave vector of the magnetic spiral in the A phase becomes oriented perpendicular to the direction of the magnetic field [61]. But the recent neutron-diffraction studies performed in a special geometry indicate, according to the authors of [9], in favor of the skyrmion-related nature of the magnetic order in the A phase. In fact, the authors of [9] speak of the observation of a two-dimensional lattice of skyrmion vortices, which can be represented as a superposition of three spirals arranged at an angle of 120° and located in a plane perpendicular to the magnetic field vector [8, 62]. The corresponding measurements performed in [63] using solid solutions $Mn_{1-x}Fe_xSi$, $Mn_{1-x}Co_xSi$, and $Fe_{1-x}Co_xSi$, which crystallize, just as MnSi, in the B20-type structure, led these authors to analogous conclusions. Finally, the direct observations of a skyrmion lattice in $Fe_{1-x}Co_xSi$ and FeGe performed using Lorentz electron microscopy [64, 65] should be mentioned. Nevertheless, as was noted in [65], the structural data do not allow clarifying whether the spin structure observed in the A phase is a true skyrmion crystal. It has been claimed that this problem can be solved by the investigation of the so-called topological Hall effect [66].

We note that the ideas on the formation of skyrmions in spin systems with a chiral spin–orbital interaction were first suggested in [67, 68].

Appendix II: Heat capacity and entropy of MnSi at $T > T_c$

Various contributions to the heat capacity of MnSi were analyzed based on the experimental and calculated data that characterize the phonon spectrum of MnSi [33]. Figure 24 illustrates the behavior of the heat capacity of MnSi in a zero magnetic field and in the field $B = 4$ T. We can seen that the magnetic field suppresses the phase transition, as was shown in Section 2.2 (see Figs 7 and 9). On the other hand, the heat capacity of MnSi in the magnetic field $B = 4$ T is higher than

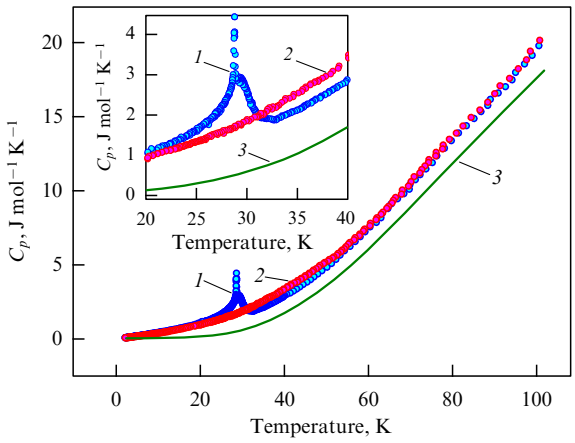

Figure 24. Heat capacity of MnSi at (*1*) $B = 0$ and (*2*) $B = 4$ T and (*3*) the calculated phonon contribution to heat capacity of MnSi.

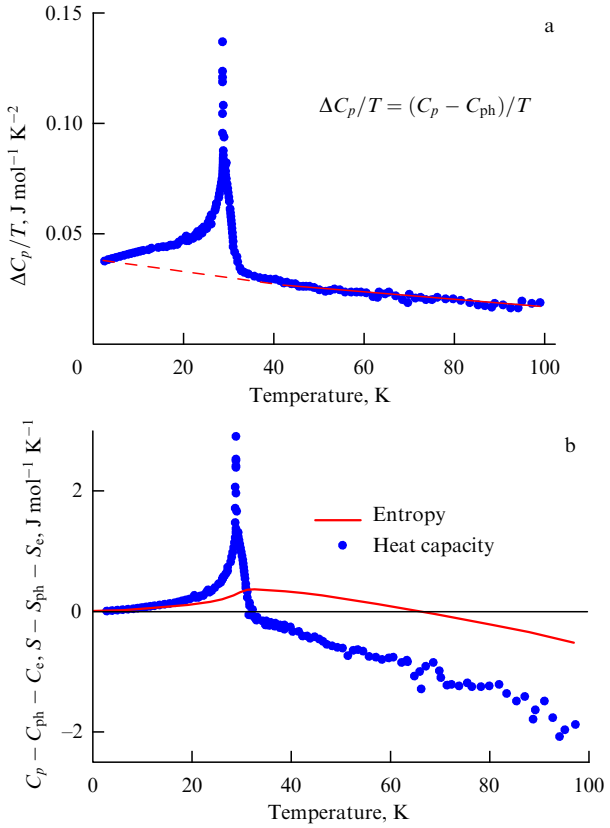

Figure 25. Temperature dependence of (a) $\Delta C_p/T = (C_p - C_{ph})/T$ ratio and (b) the 'magnetic' heat capacity and entropy for MnSi. C_{pg} is the phonon contribution.

that at $B = 0$, which seems to be somewhat strange, because the magnetic field suppresses spin fluctuations.

Figure 25 displays the temperature dependence of the ratio $\Delta C_p/T = (C_p - C_{ph})/T$, where C_{ph} is the phonon part of the heat capacity. It can be seen from the figure that the linear (electron-related) term γ in the heat capacity of MnSi has the same value at both $T < T_c$ and $T > T_c$. By subtracting the electron and phonon components from the total heat capacity, the authors of [33] came to a conclusion on the existence of negative contributions to the heat capacity and entropy of MnSi at $T > T_c$ and $B = 0$ (Fig. 25b). We recall that such a behavior of the heat capacity was predicted many years ago as a result of the existence of nonlinear effects in fluctuating spin systems [69]. The authors of [33] assume that the decrease in the partial entropy means the appearance of some ordering in the spin subsystem. However, it is impossible at present to decide whether this situation is related to the formation of skyrmion-like vortex structures or it merely reflects the tendency to spin localization.

Acknowledgments. This work was supported in part by the Russian Foundation for Basic Research (project no. 09-02-00336).

References

1. Borén B *Arkiv Kemi Min. Geol.* **11A** 1 (1933)
2. Thompson J D, Fisk Z, Lonzarich G G *Physica B* **161** 317 (1989)
3. Pfleiderer C, Julian S R, Lonzarich G G *Nature* **414** 427 (2001)
4. Doiron-Leyraud N et al. *Nature* **425** 595 (2003)
5. Pfleiderer C et al. *Nature* **427** 227 (2004)
6. Rößler U K, Bogdanov A N, Pfleiderer C *Nature* **442** 797 (2006)
7. Binz B, Vishwanath A, Aji V *Phys. Rev. Lett.* **96** 207202 (2006)
8. Tewari S, Belitz D, Kirkpatrick T R *Phys. Rev. Lett.* **96** 047207 (2006)
9. Mühlbauer S et al. *Science* **323** 915 (2009)
10. Tanaka M et al. *J. Phys. Soc. Jpn.* **54** 2970 (1985)
11. Ishida M et al. *J. Phys. Soc. Jpn.* **54** 2975 (1985)
12. Williams H J et al. *J. Appl. Phys.* **37** 1256 (1966)
13. Ishikawa Y et al. *Solid State Commun.* **19** 525 (1976)
14. Dzyaloshinsky I *J. Phys. Chem. Solids* **4** 241 (1958)
15. Moriya T *Phys. Rev.* **120** 91 (1960)
16. Kataoka M et al. *J. Phys. Soc. Jpn.* **53** 3624 (1984)
17. Grigoriev S V et al. *Phys. Rev. B* **81** 012408 (2010)
18. Petrova A E et al. *Phys. Rev. B* **82** 155124 (2010)
19. Jeong T, Pickett W E *Phys. Rev. B* **70** 075114 (2004)
20. Pan Z J, Zhang L T, Wu J S *J. Appl. Phys.* **101** 033715 (2007)
21. Mattheiss L F, Hamann D R *Phys. Rev. B* **47** 13114 (1993)
22. Wernick J H, Wertheim G K, Sherwood R C *Mat. Res. Bull.* **7** 1431 (1972)
23. Fawcett E, Maita J P, Wernick J H *Int. J. Magnetism* **1** 29 (1970)
24. Thessieu C et al. *Solid State Commun.* **95** 707 (1995)
25. Petrova A E et al. *Phys. Rev. B* **74** 092401 (2006)
26. Pfleiderer C *J. Magn. Magn. Mater.* **226–230** 23 (2001)
27. Stishov S M et al. *Phys. Rev. B* **76** 052405 (2007)
28. Ishikawa Y, Komatsubara T, Bloch D *Physica B* **86–88** 401 (1977)
29. Ishikawa Y, Arai M *J. Phys. Soc. Jpn.* **53** 2726 (1984)
30. Stishov S M et al. *J. Phys. Condens. Matter* **20** 235222 (2008)
31. Lamago D et al. *Physica B* **385–386** 385 (2006)
32. Bak P, Jensen M H *J. Phys. C* **13** L881 (1980)
33. Stishov S M et al. *Phys. Rev. Lett.* **105** 236403 (2010)
34. Belitz D, Kirkpatrick T R, Rosch A *Phys. Rev. B* **73** 054431 (2006)
35. Janoschek M et al. *Phys. Rev. B* **81** 214436 (2010)
36. Matsunaga M, Ishikawa Y, Nakajima T *J. Phys. Soc. Jpn.* **51** 1153 (1982)
37. Petrova A E, Stishov S M *J. Phys. Condens. Matter* **21** 196001 (2009)
38. Petrova A E, Stishov S M *Prib. Tekh. Eksp.* (4) 173 (2009) [*Instrum. Exp. Tech.* **52** 609 (2009)]
39. Kusaka S et al. *Solid State Commun.* **20** 925 (1976)
40. Nakanishi O et al. *Solid State Commun.* **35** 995 (1980)
41. Diep H T *Phys. Rev. B* **39** 397 (1989)
42. Plumer M L, Mailhot A *Phys. Rev. B* **50** 16113 (1994)
43. Pappas C et al. *Phys. Rev. Lett.* **102** 197202 (2009)
44. Pfleiderer C, McMullan G J, Lonzarich G G *Physica B* **206–207** 847 (1995)
45. Pfleiderer C et al. *Phys. Rev. B* **55** 8330 (1997)
46. Pfleiderer C et al. *Physica B* **230–232** 576 (1997)
47. Thessieu C, Pfleiderer C, Flouquet J *Physica B* **239** 67 (1997)
48. Thessieu C, Kitaoka Y, Asayama K *Physica B* **259–261** 847 (1999)
49. Belitz D, Kirkpatrick T R, Vojta T *Phys. Rev. Lett.* **82** 4707 (1999)
50. Petrova A E et al. *Phys. Rev. B* **79** 100401(R) (2009)
51. Miyake A et al. *J. Phys. Soc. Jpn.* **78** 044703 (2009)
52. Pfleiderer C et al. *Science* **316** 1871 (2007)
53. Pedrazzini P et al. *Physica B* **378–380** 165 (2006)

54. Ford P J, Mydosh J A *Phys. Rev. B* **14** 2057 (1976)
55. Kirkpatrick T R, Belitz D *Phys. Rev. Lett.* **104** 256404 (2010)
56. Uemura Y J et al. *Nature Phys.* **3** 29 (2007)
57. Yu W et al. *Phys. Rev. Lett.* **92** 086403 (2004)
58. Andreica D et al. *Phys. Rev. B* **81** 060412(R) (2010)
59. Lebech B, in *Recent Advances in Magnetism of Transition Metal Compounds* (Eds A Kotani, N Suzuki) (Singapore: World Scientific, 1993) p. 167
60. Lebech B et al. *J. Magn. Magn. Mater.* **140 – 144** 119 (1995)
61. Grigoriev S V et al. *Phys. Rev. B* **73** 224440 (2006)
62. Binz B, Vishwanath A *Phys. Rev. B* **74** 214408 (2006)
63. Münzer W et al. *Phys. Rev. B* **81** 041203(R) (2010)
64. Yu X Z et al. *Nature* **465** 901 (2010)
65. Yu X Z et al. *Nature Mater.* **10** 106 (2011)
66. Neubauer A et al. *Phys. Rev. Lett.* **102** 186602 (2009)
67. Bogdanov A N, Yablonskii D A *Zh. Eksp. Teor. Fiz.* **95** 178 (1989) [*Sov. Phys. JETP* **68** 101 (1989)]
68. Bogdanov A, Hubert A *J. Magn. Magn. Mater.* **138** 255 (1994)
69. Murata K, Doniach S *Phys. Rev. Lett.* **29** 285 (1972)